Rational design of Fe/Co-based diatomic catalysts for Li–S batteries by first-principles calculations

Xiaoya Zhang(张晓雅)[1], Yingjie Cheng(程莹洁)[1], Chunyu Zhao(赵春宇)[1], Jingwan Gao(高敬莞)[1], Dongxiao Kan(阚东晓)[2,†], Yizhan Wang(王义展)[1], Duo Qi(齐舵)[3], and Yingjin Wei(魏英进)[1,‡]

[1] *Key Laboratory of Physics and Technology for Advanced Batteries (Ministry of Education), College of Physics, Jilin University, Changchun* 130012, *China*
[2] *Advanced Materials Research Central, Northwest Institute for Non-Ferrous Metal Research, Xi'an* 710016, *China*
[3] *College of Materials Science and Engineering, Shenyang University of Chemical Technology, Shenyang* 110142, *China*

(Received 1 November 2022; revised manuscript received 22 November 2022; accepted manuscript online 29 November 2022)

Fe/Co-based diatomic catalysts decorated on an N-doped graphene substrate are investigated by first-principles calculations to improve the electrochemical properties of Li–S batteries. Our results demonstrate that $FeCoN_8$@Gra not only possesses moderate adsorption energies towards Li_2S_n species, but also exhibits superior catalytic activity for both reduction and oxidation reactions of the sulfur cathode. Moreover, the metallic property of the diatomic catalysts can be well maintained after Li_2S_n adsorption, which could help the sulfur cathode to maintain high conductivity during the whole charge–discharge process. Given these exceptional properties, it is expected that $FeCoN_8$@Gra could be a promising diatomic catalyst for Li–S batteries and afford insights for further development of advanced Li–S batteries.

Keywords: Li–S battery, diatomic catalyst, polysulfides, first-principles calculations

PACS: 68.43.Bc, 82.45.Jn, 88.80.ff **DOI:** 10.1088/1674-1056/aca6da

1. Introduction

The thriving development of electric vehicles and handheld electronics demands secondary batteries with high energy density and long cycle life. The application of lithium-ion batteries in these fields is seriously hindered by the limited theoretical energy density. So, novel electrode materials or alternative technologies are highly desired.[1,2] Lithium–sulfur (Li–S) battery has been regarded as a promising alternative to traditional lithium-ion batteries due to its high energy density and low cost of sulfur. However, the practical application of Li–S battery has faced big challenges of the shuttling effect and sluggish conversion kinetics of polysulfides (Li_2S_n) and poor electronic conductivity of S.[3–6] To address these issues, carbon-based materials,[7–9] transition metal (TM) oxides (or sulfides, nitrides)[10,11] has been developed as the S cathode hosts to restrict Li_2S_n shuttling, improve the conductivity and enhance redox kinetics. Especially, due to the favorable transportation of both electrons and Li-ions, graphene has been wildly studied as S cathode host. However, polysulfides can only be adsorbed on graphene via a weak van der Waals (vdW) bond, which results in weak anchoring ability and poor catalytic activity. Some studies used N- or B-doped graphene to anchor Li_2S_n and catalyze Li_2S_n conversion.[12,13] But the improved anchoring and catalytic effects were mainly attributed to the "Li-bond" between Li_2S_n and the non-metallic atoms, while no "S-bond" was formed due to the absence of metal atoms.[14]

To better inhibit the shuttling effect and promote the conversion of Li_2S_n, it has been proposed to decorate single atom of TMs on graphene as single atom catalysts (SACs) for Li–S batteries.[15,16] The adsorption and conversion of Li_2S_n can be effectively facilitated via the synergy of Li-bond and S-bond between the adsorbents and the SACs, thus improving the cycling performance of the batteries. Fe, Co, Ni, and V SACs decorated on N-doped graphene have been studied, in which the Fe and Co-based SACs have shown promising bifunctional activity for sulfur reduction (SRR) and sulfur oxidation (SER) reactions of the sulfur cathode.[17–19] Nevertheless, the adsorption of Li_2S_n on the SACs is still weak especially for long chain Li_2S_n ($n > 4$) due to the lack of S-bond caused by the limited TM atoms on graphene (usually less than 1.5 at.%), which further hindered the catalytic performance of the SACs.[20]

Recently, as a further extension of SACs, diatomic catalysts (DACs)[21] have shown promising catalytic effect for many electrochemical processes such as oxygen reduction reaction (ORR), oxygen evolution reaction (OER), hydrogen evolution reaction (HER), NO_x reduction reaction (NO_xRR), and CO_2 reduction reaction due to their increased active sites and improved catalytic mechanism.[22–27] Lu *et al.* demonstrated that the graphene-supported Pt_2 dimer was approximately 17 times more active than single-atom Pt_1 during the hydrogen evolution reaction,[28] Based on these significant advantages, it can be inferred that the electrochemical properties of Li–S batteries can be effectively improved by using a proper

†Corresponding author. E-mail: dxkan1202@126.com
‡Corresponding author. E-mail: yjwei@jlu.edu.cn

© 2023 Chinese Physical Society and IOP Publishing Ltd

DAC. However, no DAC has been applied in Li–S batteries to date. Considering Fe and Co-based SACs have been proven as promising catalysts for Li–S batteries, herein we construct a series of Fe and Co-based DACs on an N-doped graphene substrate via first-principles calculations, which are denoted as $M_1M_2N_x$@Gra, where M_1M_2 represent different Fe and Co diatomic couples, x is the coordination number of N with M_1 or M_2. Based on systematical evaluation of anchoring ability and catalytic behavior, $FeCoN_8$@Gra is screened as a promising bifunctional DAC for Li–S batteries which shows more effective catalytic ability than its SAC counterparts.

2. Calculation methods

All first-principles calculations were performed using the Vienna *ab initio* simulation package (VASP).[29] The Perdew–Burke–Ernzerhof exchange–correlation function in the scheme of generalized gradient approximation was used for electron exchange–correlation interactions, and the projector-augmented-wave potentials were used to consider electron–ion interactions.[30] The electron wave functions were expanded in a plane wave basis with a kinetic energy cutoff of 500 eV, a $3\times3\times1$ Monkhorst–Pack k-mesh was used for sampling Brillouin zones, and $5\times5\times1$ for electronic density of states (DOS) and Bader charge calculations.[31] The optimized lattice constants of DACs are 25 Å. The DACs were set in a 8×8 supercell of graphene and the vacuum thickness was set as 15 Å to avoid interlayer interactions. All the atomic positions and lattice vectors were fully optimized using a conjugate gradient algorithm to obtain an unstrained configuration. Atomic relaxation was performed until the change in total energy was less than 1×10^{-5} eV, and the maximum forces were smaller than 0.02 eV/Å. Thermodynamic stability of the substrates were evaluated by molecular dynamics (MD) simulations, where NVT ensemble was lasted for 3 ps with a time step of 1.0 fs. The DFT-D3 function including the vdW interaction as well as spin polarization correction was considered in simulations. Moreover, the partial density of states (PDOS) and Bader charge of the Li_2S_n adsorbed systems were calculated to study the adsorption effect and charge transfer between $M_1M_2N_x$@Gra and Li_2S_n.

Formation energies (E_{form}) were calculated by the following formula:[24]

$$E_{form} = E_{M_1M_2N_x\text{-Gra}} + y\mu_c - E_{Gra} - \mu_{M_1} - \mu_{M_2} - x\mu_N, \quad (1)$$

where $E_{M_1M_2N_x\text{-Gra}}$ and E_{Gra} are the total energies of $M_1M_2N_x$@Gra and graphene, respectively. μ_c is the chemical potential of a single C atom in graphene, μ_N is the chemical potential of one N atom from the gas phase N_2 molecule, μ_{M_1} and μ_{M_2} are the energies of isolated M_1 and M_2 atoms, and x is the coordination number of N with M_1 or M_2, y is the number of removed C atoms. The adsorption energy (E_{ad}) of Li_2S_n on $M_1M_2N_x$@Gra is defined as the energy difference between the adsorbed system (E_{tot}) and the summation of individual Li_2S_n ($E_{molecule}$) and $M_1M_2N_x$@Gra (E_{host}), which was expressed as

$$E_{ad} = E_{molecule} + E_{host} - E_{tot}. \quad (2)$$

The differential charge density analysis by the following equation:[32]

$$\Delta\rho = \rho_{sub+ps} - \rho_{sub} - \rho_{ps}, \quad (3)$$

where ρ_{sub+ps}, ρ_{sub}, and ρ_{ps} represent the charge densities of the DACs with various polysulfides, pristine DACs, and the polysulfides, respectively. In addition, the reactions of SRR for the conversions of Li_2S_n/S_8 are listed in Eqs. (4)–(8), where the asterisk $*$ stands for an active site on the catalytic surface:[33]

$$^*S_8 + 2Li + +2e^- \rightarrow {}^*Li_2S_8, \quad (4)$$

$$^*Li_2S_8 \rightarrow {}^*Li_2S_6 + 1/4S_8, \quad (5)$$

$$^*Li_2S_6 \rightarrow {}^*Li_2S_4 + 1/4S_8, \quad (6)$$

$$^*Li_2S_4 \rightarrow {}^*Li_2S_2 + 1/4S_8, \quad (7)$$

$$^*Li_2S_2 \rightarrow {}^*Li_2S + 1/8S_8. \quad (8)$$

The free energy of each SRR step was calculated by the following equation:[34]

$$\Delta G = \Delta E_{tot} + \Delta E_{ZPE} - TS, \quad (9)$$

where ΔE_{tot} is the total energy, $T = 298.15$ K is room temperature, S is the entropy, ΔE_{ZPE} is the zero-point energy. $\Delta E_{ZPE} - TS$ is determined by calculating the vibrational frequencies of the adsorbed intermediates using the partial hessian method.

3. Results and discussion

3.1. The polysulfides anchoring ability of $M_1M_2N_x$@Gra

In this study, two DAC models were proposed based on the previous works of Fe and Co-based SACs.[19,20] One is $M_1M_2N_6$@Gra where the TMs are coordinated to six N atoms and the other is $M_1M_2N_8$@Gra where the TMs are coordinated to eight N atoms. Accordingly, six DACs were got: $FeCoN_6$@Gra, Fe_2N_6@Gra, Co_2N_6@Gra, Fe_2N_8@Gra, Co_2N_8@Gra, and $FeCoN_8$@Gra, with their optimized structures displayed in Figs. 1(a) and S1(a). All these DACs show negative formation energies (Table 1), indicating thermodynamic stability of the structures. Apart from the different coordination numbers, another big difference between the two DAC models lies in the distance between M_1 and M_2 ($d_{m_1-m_2}$), where the $d_{m_1-m_2}$ of $M_1M_2N_6$@Gra (~ 2.20 Å) is obviously smaller than that of $M_1M_2N_8$@Gra (~ 4.10 Å), with binding energies ranging from -5.93 eV (Fe_2N_8@Gra) to -7.95 eV (Co_2N_6@Gra). Furthermore, MD simulations were performed

at 300 K to determine the thermodynamic stability of these DACs. All the six structures remain basically stable after 3-ps simulation and the fluctuation range of the total energy are less and less over time (Figs. 1(b) and S1(b)), which further proves their structural stability at room temperature.

The electronic properties of the DACs were studied by electron local function (ELF). For all the DACs, the charges are mostly localized on the N atom, whereas no charge distribution is found around Fe or Co, implying the ionic bonding (Fig. S2(a)). There is an obvious light-blue region between the TM atoms in $M_1M_2N_6$@Gra, which is attributed to electrons overlap of M_1 and M_2 due to the short M_1–M_2 distance. In contrast, there is no electrons overlap in $M_1M_2N_8$@Gra due to the long M_1–M_2 distance. Figure 1(c) shows the calculated DOS of the $FeCoN_8$@Gra and $FeCoN_6$@Gra. Compared to the bare N_6@Gra and N_8@Gra substrates, all the $M_1M_2N_6$@Gra and $M_1M_2N_8$@Gra structures show metallic features where the electronic states at the Fermi level are mainly from Fe/Co-3d (Fig. S2(b)). This indicates all the DACs have good electronic conductivity, which is important to accelerate the electrochemical reactions of Li–S batteries.

Table 1. The distance between the metal atoms in the substrate (d_{m1-m2} in unit Å) and the formation energy of the substrate (E_F in unit eV).

	Co_2N_6	$FeCoN_6$	Fe_2N_6	Co_2N_8	$FeCoN_8$	Fe_2N_8
d_{m1-m2} (Å)	2.23	2.17	2.21	4.10	4.11	4.11
E_F (eV)	−7.95	−7.48	−6.54	−6.58	−6.24	−5.93

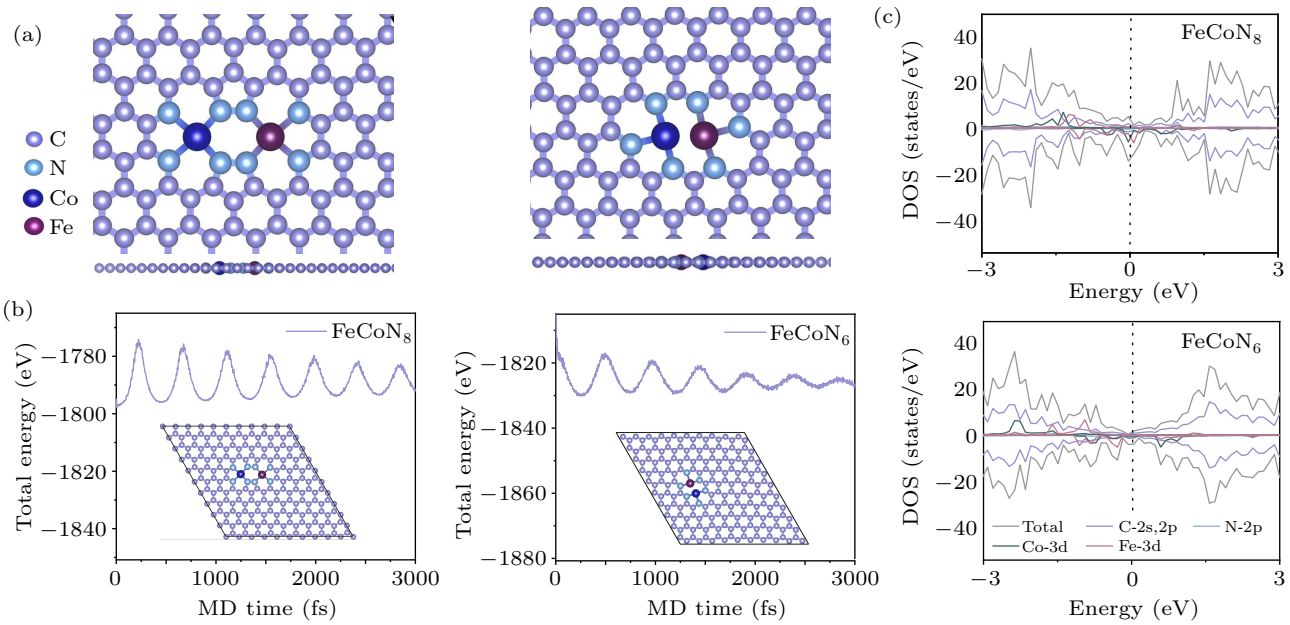


Fig. 1. (a) Crystal structures of $FeCoN_8$@Gra (left) and $FeCoN_6$@Gra (right) from top and side views. (b) Molecular dynamics simulations. (c) Total and partial density of states of $FeCoN_8$@Gra and $FeCoN_6$@Gra.

The adsorption energy (E_{ad}) of polysulfides is a critical factor for evaluating the anchoring ability of the catalyst. Figure 2(a) shows the energetically favorable adsorption configurations of S_8 and Li_2S_n (n = 1, 2, 4, 6, 8) on $FeCoN_8$@Gra. It can be seen that all the adsorbents can be stably adsorbed without significant structural deformation. In addition, the adsorbents form Li–N and Fe/Co–S bonds with $FeCoN_8$@Gra. Similar results are also obtained for the other five DACs (Fig. S3). The average Li–N bond length of $M_1M_2N_6$@Gra is longer than that of $M_1M_2N_8$@Gra by about 0.6 Å, which indicates the Li–N bond is stronger in $M_1M_2N_8$@Gra than in $M_1M_2N_6$@Gra. However, the Fe/Co–S bonds for all the six DACs are close to 2.3 Å (Table S1). For almost all the DACs, the E_{ad} gradually increased with lithiation which reached a maximum value for the fully lithiated Li_2S product, indicating the shuttling effect is mainly caused by long chain polysulfides (Fig. 2(b)). Except for Co_2N_8@Gra, the E_{ad} of Li_2S_n ($n \geq 4$) are in the range of 1.5 eV–2.8 eV. These values are much larger than those of the Co/Fe decorated N-doped graphene SACs,[35] indicating that DACs can better suppress the shuttling of Li_2S_n. The improved anchoring ability could be attributed to the more Fe/Co–S bonds of the DACs, due to the doubled TM sites compared to their SAC counterparts. Moreover, all these E_{ad} values are much larger than those of 1,3-dioxolane (DOL) (*e.g.*, 0.75 eV for Li_2S_6) and 1,2-dimethoxyethane (DME) (*e.g.*, 0.77 eV for Li_2S_6) electrolyte solvents.[10] This indicates that the DACs can not only anchor the polysulfides in the S cathode, but also can capture the dissolved polysulfides from the electrolyte. These advantages can effectively improve the cycle stability of Li–S batteries, resulting in prolonged cycle life.

Charge density difference (CDD) analysis was performed to further reveal the anchoring mechanism of the DACs. The CDD patterns in Fig. 2(c) clearly show the formation of Fe/Co–S and Li–N bonds, taking Li_2S_2 as example. The in-

ternal charge loss of Li_2S_2 (blue part) leads to softening of the Li–S bond, which is confirmed by the elongation of the Li–S bond from 2.21 Å (in vacuum) to 2.55 Å (absorbed on $FeCoN_8$@Gra), which is conducive to the conversion of polysulfides. Additionally, Bader charge analyses were performed to quantitatively describe the charge transfer between Li_2S_n and the DACs. Taken $FeCoN_8$@Gra in detail, the corresponding charge transfer value is $0.17|e|$ for S_8, $0.11|e|$ for Li_2S_8, $0.25|e|$ for Li_2S_6, $0.41|e|$ for Li_2S_4, $0.62|e|$ for Li_2S_2, and $0.72|e|$ for Li_2S. The gradually increased charge transfer implies stronger adsorption of Li_2S_n on $FeCoN_8$@Gra with lithiation (Fig. 2(d)), which proves that the DACs can effectively absorb polysulfides.

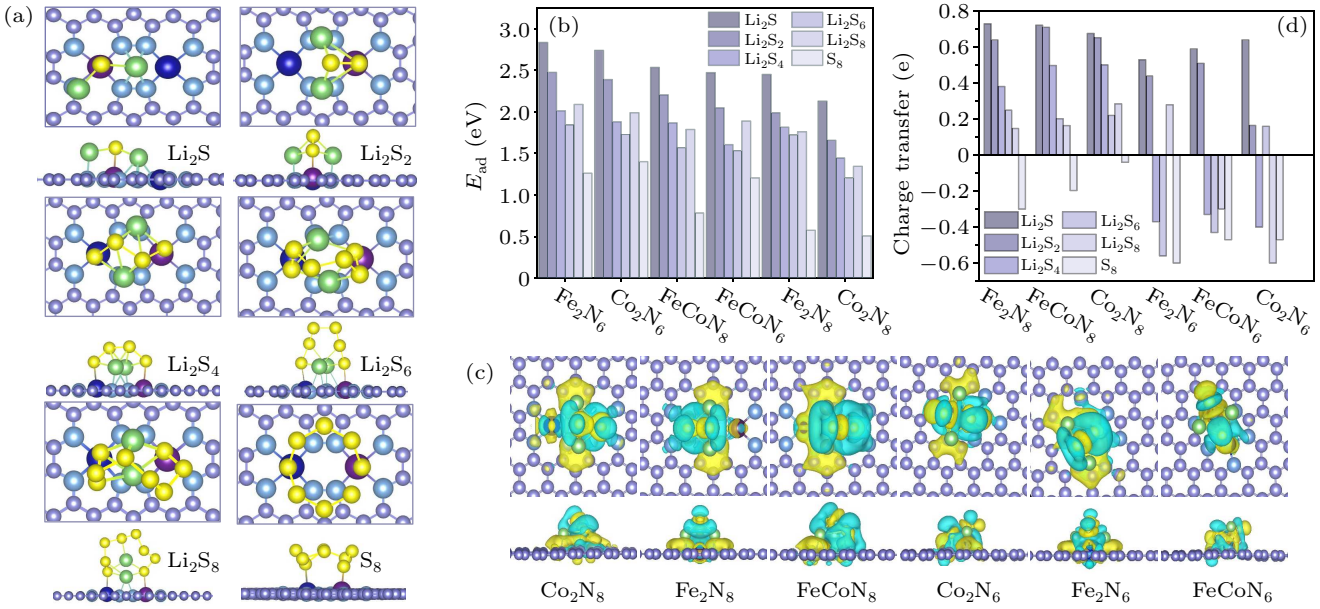


Fig. 2. (a) The energetically favorable absorption structures of S_8 and Li_2S_n (n = 1,2,4,6,8) on $FeCoN_8$@Gra. (b) Adsorption energy of S_8/Li_2S_n on DACs. (c) Charge density difference for Li_2S_2 on substrates, yellow (green) is the spatial regions that gain (loss) in charge. (d) Charge transfer between S_8/Li_2S_n and DACs. Li: green, S: yellow, C: lilac, N: light blue, Fe: purple, and Co: dark blue. The iso-surface level is 0.001 e·Å^{-3}.

3.2. The catalytic properties of $M_1M_2N_x$@Gra

The overall SRR process (*i.e.*, the discharge of Li–S battery) catalyzed with the $M_1M_2N_x$@Gra DACs was then studied. Generally, the lithiation process follows a sequence of reactions including an initial exothermic reaction from S_8 to Li_2S_8, then the Li_2S_8 cluster is gradually reduced to the soluble intermediates of Li_2S_6 and Li_2S_4, which further transforms into Li_2S_2 and Li_2S solids (Eqs. (4)–(8)). The sluggish liquid–solid and solid–solid reaction kinetics not only hinder the rate capability of Li–S batteries but also lead to accumulation of the soluble intermediates, which aggravates the shuttling effect. To evaluate the catalytic ability of the DACs, we performed Gibbs free energy calculations for each elementary reaction step of SRR, and the relative energy evolution profiles from S_8 to Li_2S are shown in Fig. 3(a).[36] Tables S2 and S3 respectively presents the calculation details of free energy and ΔG of each basic reaction step of SRR. In all the reaction steps, $Li_2S_4 \rightarrow Li_2S_2$ has the largest ΔG and is the rate-limiting step of the SRR process. To further reveal the relationship between the catalytic effect and the adsorption properties, the ΔG of the $Li_2S_4 \rightarrow Li_2S_2$ step and the E_{ad} of Li_2S_2 on the DACs are plotted in Fig. 3(b). This relationship reflects a volcano-like feature, where $FeCoN_8$@Gra shows the lowest ΔG of 0.62 eV at a moderate E_{ad} of 2.2 eV. This Gibbs free energy is also smaller than those of the SACs of Co (1.05 eV)[37] or Fe (1.4 eV)[17] decorated N-doped graphene, indicating the $FeCoN_8$@Gra DAC can better catalyze the conversion reactions of Li–S batteries.

Furthermore, the specific dissociation energy of Li_2S (*i.e.*, $Li_2S \rightarrow LiS + Li^+ + e^-$) was calculated to study the dynamic properties of the SER process[38] (*i.e.*, the charge process of Li–S battery). The dissociation energy ΔE_{ad} follows the formula $\Delta E_{ad} = E_{*Li2S} - E_{*LiS} - E_{Li}$, where E_{*Li2S} (E_{*LiS}) is the adsorbed system of DACs and molecule of Li_2S (LiS), E_{Li} is the energy of Li atom in bulk.[39] As shown in Fig. 3(c), compared to the primitive Li_2S molecular whose dissociation energy is as high as 3.04 eV, the DACs can significantly reduce the dissociation energy of Li_2S, especially for $FeCoN_8$@Gra (0.517 eV) and Co_2N_6@Gra (0.506 eV). These results are also much smaller than those of the CoN_4@Gra (1.37 eV)[17] and FeN_4@Gra (1.5 eV) SACs.[39] Based on the above discussion, $FeCoN_8$@Gra can be used as a promising bifunctional DAC due to its greatly improved SRR and SER kinetics compared to the other five DACs and reported SACs.[19,33]

PDOS analysis was performed to further reveal the catalytic mechanism of the DACs, taking Li_2S_2 as a typical adsorbent. Figure 4(a) shows the PDOS of the Li_2S_2 adsorbed $FeCoN_8$@Gra system (denoted as $FeCoN_8$@Gra–Li_2S_2). Meanwhile, the PDOS of other cases are provided

in Fig. S4, which presents similar results. The S-2p orbitals and Co/Fe-3d orbitals have significant hybridization near the Fermi level, indicating a strong S-bond formed between the $FeCoN_8$@Gra DAC and the Li_2S_2 adsorbent. In comparison, the hybridization of Li-2s and N-2p orbitals is slight. This phenomenon proves that the Li-bond of the adsorbed system is relatively weak, and the S-bond plays a key role in the polysulfide anchoring mechanism. The Fe/Co-3d PDOS of the Li_2S_2 absorbed DACs is shown in Fig. S5. It clearly shows the Fe/Co-3d states become broader after Li_2S_2 adsorbed on the DACs due to the interaction between Fe/Co and S. In addition, the Fe-3d state is more diffuse compared to the Co-3d state, which indicates stronger interaction between Fe and S due to the large electronegativity difference. Moreover, bare Li_2S_2 is known as an electronic insulator. The $FeCoN_8$@Gra–Li_2S_2 system, however, shows considerable electronic states at the Fermi level. This indicates that the DACs can help the S cathode maintain high electronic conductivity during the whole charge–discharge process, which could significantly improve the cycling performance of Li–S batteries.

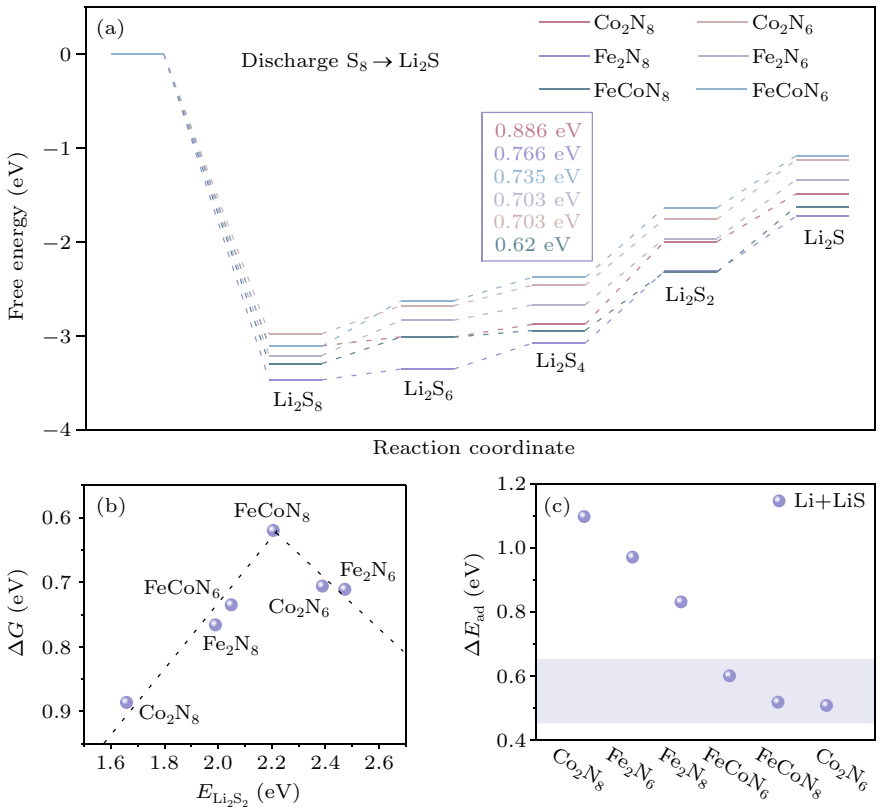


Fig. 3. (a) Calculated Gibbs free energy diagram of $M_1M_2N_6$@Gra and $M_1M_2N_8$@Gra for the SRR process, (b) the relationship between the Gibbs free energy of the rate limiting step and the E_{ad} of Li_2S_2 on the DACs, (c) the decomposition energy of $Li_2S \rightarrow Li + LiS$ on the DACs.

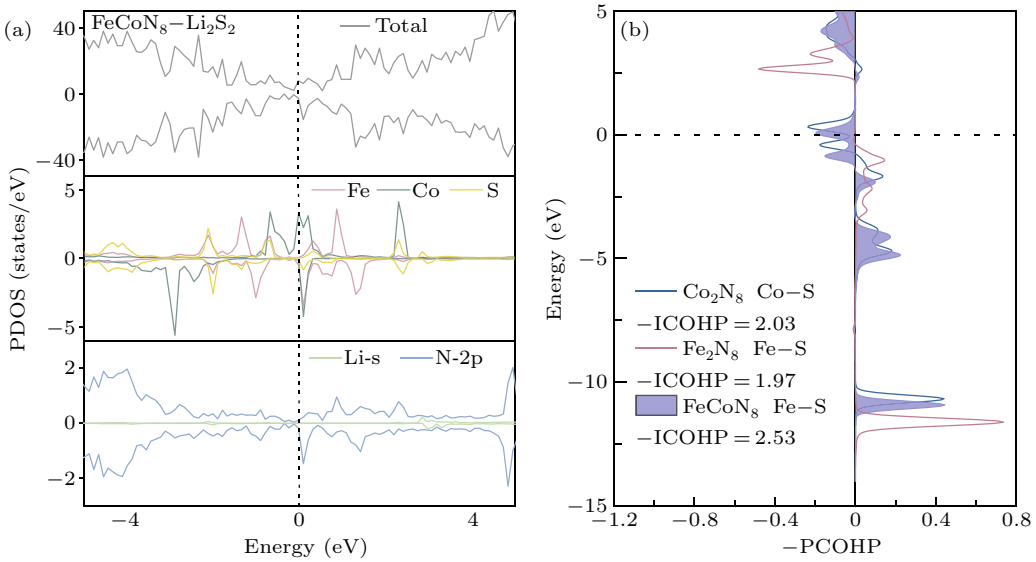


Fig. 4. (a) Calculated DOS of $FeCoN_8$@Gra–Li_2S_2, (b) COHP diagram of the Fe/Co–S bond in Li_2S_2 on Co_2N_8@Gra (blue line), Fe_2N_8@Gra (pink line), and $FeCoN_8$@Gra (purple shade).

Furthermore, crystal orbital hamilton population (COHP) analysis was introduced to explore the bonding strength of Fe/Co–S (Fig. 4(b)). Compared to Co_2N_8@Gra–Li_2S_2 and Fe_2N_8@Gra–Li_2S_2, the proportion of bonding states of the Fe–S bond in $FeCoN_8$@Gra–Li_2S_2 below the Fermi level is significantly increased with a -ICOHP value of 2.53. This indicates the synergistic interaction between Fe and Co can enhance the S bonding strength, which is consistent with the trend in the calculated adsorption energies. Benefiting from the high electronic conductivity and excellent bifunctional catalytic ability, $FeCoN_8$@Gra can effectively accelerate the Li_2S_n conversion reaction and improve the electrode kinetics of Li–S batteries.

4. Conclusion

In conclusion, Fe/Co-based DACs for Li–S batteries were systematically studied by first-principles calculations. All the DACs showed negative formation energy indicating thermodynamic stability of their structures. The adsorption energies for polysulfides were much larger than their SAC counterparts and DOL/DME solvents without significant structural deformation, highlighting the excellent anchoring ability of the DACs. Also, metallic properties of the bare and polysulfides adsorbed DACs conferred high conductivity of the S cathode during the whole charge–discharge process. Among all the DACs under investigation, $FeCoN_8$@Gra exhibited promising bifunctional catalytic activity with low energy barriers for both SRR and SER processes, which can effectively accelerate the Li_2S_n conversion reactions, guarantee high sulfur utilization and long cycling stability. This study provides a theoretical guidance for future experimental studies of Li–S batteries in exploring promising diatomic catalysts.

Acknowledgments

Project supported by the National Natural Science Foundation of China (Grant Nos. 51972140 and 51903164) and the Fund from Science and Technology Department of Jilin Province, China (Grant No. 20200201069JC).

References

[1] Liu W, Liu W, Li X, Liu Y, Ogunmoroti A E, Li M, Bi M and Cui Z 2021 *Resour. Conserv. Recycl.* **164** 105122
[2] Nitta N, Wu F, Lee J T and Yushin G 2015 *Mater. Today* **18** 252
[3] Manthiram A, Fu Y, Chung S H, Zu C and Su Y S 2014 *Chem. Rev.* **114** 11751
[4] Peng H J, Huang J Q, Cheng X B and Zhang Q 2017 *Adv. Energy Mater.* **7** 1700260
[5] Liu D, Zhang C, Zhou G, Ling W Lv G, Zhi L and Yang Q H 2018 *Adv. Sci.* **5** 1700270
[6] Yin Y X, Yao H R and Guo Y G 2016 *Chin. Phys. B* **25** 018801
[7] Zhao J, Sun H, Dai S, Wang Y and Zhu J 2011 *Nano Lett.* **11** 4647
[8] Zheng G, Yang Y, Cha J J, Hong S S and Cui Y 2011 *Nano Lett.* **11** 4462
[9] Chen H L, Xiao Z J, Zhang N, Xiao S Q, Xia X G, Xi W, Wang Y C, Zhou W Y and Xie S S 2018 *Chin. Phys. B* **27** 068101
[10] Wang D, Zhao S, Li F, He L, Zhao Y, Zhao H, Liu Y, Wei Y and Chen G 2019 *ChemSusChem* **12** 4671
[11] Wang Z, Niu X, Xiao J, Wang C, Liu J and Gao F 2013 *RSC Adv.* **3** 16775
[12] Xie Y, Meng Z, Cai T and Han W Q 2015 *ACS Appl. Mater.* **7** 25202
[13] Wang D, Li F, Lian R, Xu J, Kan D, Liu Y, Chen G, Gogotsi Y and Wei Y 2019 *ACS Nano* **13** 11078
[14] Chen X, Bai Y K, Zhao C Z, Shen X and Zhang Q 2020 *Angew. Chem. Int. Ed.* **59** 11192
[15] Han X, Zhang Z and Xu X 2021 *J. Mater. Chem. A* **9** 12225
[16] Zhou G, Zhao S, Wang T, Yang S Z, Johannessen B, Chen H, Liu C, Ye Y, Wu Y, Peng Y, Liu C, Jiang S P, Zhang Q and Cui Y 2020 *Nano Lett.* **20** 1252
[17] Du Z, Chen X, Hu W, Chuang C, Xie S, Hu A, Yan W, Kong X, Wu X, Ji H and Wan L J 2019 *J. Am. Chem. Soc.* **141** 3977
[18] Lin Q, Ding B, Chen S, Li P, Li Z, Shi Y, Dou H and Zhang X 2020 *ACS Appl. Energy Mater.* **3** 11206
[19] Ma C, Zhang Y, Feng Y, Wang N, Zhou L, Liang C, Chen L, Lai Y, Ji X, Yan C and Wei W 2021 *Adv. Mater.* **33** 2100171
[20] Ji S, Chen Y, Wang X, Zhang Z, Wang D and Li Y 2020 *Chem. Rev.* **120** 11900
[21] Zhang J, Huang Q A, Wang J, Wang J, Zhang J and Zhao Y 2020 *Chin. J. Catal.* **41** 783
[22] Zhang L, Si R, Liu H, Chen N, Wang Q, Adair K, Wang Z, Chen J, Song Z, Li J, Banis M N, Li R, Sham T K, Gu M, Liu L M, Botton G A and Sun X 2019 *Nat. Commun.* **10** 4936
[23] Sun B, He D, Wang H B, Liu J C, Ke Z J, Cheng L and Xiao X H 2021 *Chin. Phys. B* **30** 106102
[24] Meng Y, Li K, Xiao D, Yuan Y, Wang Y and Wu Z 2020 *Int. J. Hydrog.* **45** 14311
[25] Hunter M A, Fischer J M T A, Yuan Q, Hankel M and Searles D J 2019 *ACS Catal.* **9** 7660
[26] Yang L, Ma X, Xu Y Y, Xu J Y and Song Y D 2020 *Int. J. Electrochem. Sci.* **15** 9698
[27] Lv P, Wu D H, He B L, Li X, Zhu R, Tang G, Lu Z S, Ma D W and Jia Y 2022 *J. Mater. Chem. A* **10** 9707
[28] Li H L, Wang L B, Dai Y Z, Pu Z T, Lao Z H, Chen Y W, Wang M L, Zheng X S, Zhu J F, Zhang W H, Si R, Ma C and Zeng J 2018 *Nat. Nanotechnol.* **13** 411
[29] Kresse G and Furthmüller J 1996 *Phys. Rev. B* **54** 11169
[30] Perdew J, Chevary J, Vosko S, Jackson K, Pederson, Singh D and Fiolhais C 1992 *Phys. Rev. B* **46** 6671
[31] Chadi D J 1976 *Phys. Rev. B* **13** 5188
[32] Zhang J, Huang Q A, Wang J, Wang J, Zhang J and Zhao Y 2018 *J. Mater. Chem. A* **6** 2107
[33] Ma D, Wang Y, Liu L and Jia Y 2021 *Phys. Chem. Chem. Phys.* **23** 4018
[34] Xiao W S, He Q and Zhao Y 2021 *Appl. Surf. Sci.* **570** 151213
[35] Zeng Q W, Hu R M, Chen Z B and Shang J X 2019 *Mater. Res. Express* **6** 095620
[36] Lei B, Zhang Y Y and Du S X 2020 *Chin. Phys. B* **29** 058104
[37] Zhao C, Xu G L, Yu Z, Zhang L, Wang I H, Mo Y X, Ren Y, Cheng L, Sun C J, Ren Y, Zuo X, Li J T, Sun S G, Amine K and Zhao T 2020 *Nat. Nanotechnol.* **16** 166
[38] Xiao J, Hu J Z, Chen H, Vijayakumar M, Zheng J, Pan H, Walter E D, Hu M, Deng X, Feng J, Liaw B Y, Gu M, Deng Z D, Lu D, Xu S, Wang C and Liu J 2015 *Nano Lett.* **15** 3309
[39] Zhang L, Liang P, Shu H B, Man X L, Du X Q, Chao D L, Liu Z G, Sun Y P, Wan H Z and Wang H 2018 *J. Colloid Interface Sci.* **529** 426